Tellus (2006), 58B, 206–217
Printed in Singapore. All rights reserved

TELLUS

Dehydration in the northern hemisphere mid-latitude tropopause region observed during STREAM 1998

By FARAHNAZ KHOSRAWI[1,2]*, ROLF MÜLLER[1], JÜRGEN BEUERMANN[1], PAUL KONOPKA[1] and CORNELIUS SCHILLER[1], [1]*ICG-I:Stratosphere, Forschungszentrum Jülich, D-52425 Jülich, Germany;* [2]*MISU/ITM, Stockholm University, S-106 91 Stockholm, Sweden*

(Manuscript received 14 January 2005; in final form 9 January 2006)

ABSTRACT

Measurements in the vicinity of the polar jet stream during the STREAM 1998 campaign in Timmins, Canada, show that during the flight on 15 July, a deep intrusion of stratospheric air into the troposphere occurred. At the edge of the deep intrusion dehydration was observed. The dehydration can be identified in tracer–tracer correlations of H_2O and O_3 and by the comparison of these correlations with correlations of H_2O and O_3 derived from two other flights of the STREAM 1998 campaign. Trajectories, calculated backwards for 10 days starting at each point of the measurement for the flight on 15 July, show that the saturation ratios required for homogeneous freezing are reached. However, box model simulations along the trajectories indicate no substantial growth of H_2SO_4/H_2O particles due to H_2O uptake. Since ice nuclei were not measured during the campaign, it cannot be precisely determined which freezing process, heterogeneous or homogeneous, is responsible for the formation of the ice particles. Most likely, both processes were involved in the formation of ice particles that led to the observed dehydration on 15 July 1998.

1. Introduction

The exchange of air masses between the stratosphere and troposphere has an important influence on chemical, dynamical and radiative processes in the atmosphere. Using the classification of Hoskins (1991), the atmosphere can be divided into three layers, the overworld, the middle world and the underworld. Isentropic layers for potential temperatures (Θ) are entirely in the stratosphere in the overworld, intersect the tropopause in the middle world and are below the tropopause in the underworld. The $\Theta =$ 380 K isentrope can be taken as the upper boundary of the middle world, which roughly coincides with the tropical tropopause. Using the terminology of Holton et al. (1995), the stratospheric part of the middle world between the tropopause and $\Theta = 380$ K is the lowermost stratosphere (LS) and the tropospheric part below is the upper troposphere (UT).

In the UT/LS region extra-tropical cross-tropopause exchange is believed to occur mainly along isentropes crossing the tropopause in the vicinity of the subtropical and polar jet streams. Stratospheric or tropospheric filaments like cut-off lows and tropopause folds can be formed through tropopause deformations (e.g. Reiter, 1975). Downward transport of stratospheric air in these filaments ultimately leads to irreversibly mixing with tropospheric air (e.g. Danielsen, 1968; Shapiro, 1980).

Correlations of long-lived trace gases show that a mixing layer exists between stratospheric and tropospheric air masses due to stratosphere–troposphere exchange. Hoor et al. (2002) identified this mixing layer using the relationship between CO and O_3. Correlations of other tracers, for example, H_2O and O_3, lead to the same conclusion (Krebsbach et al., 2005). Further, correlations of long-lived trace gases can be used to identify physicochemical changes like dehydration, denitrification and ozone loss, which are evident in measurements at a particular point in time (e.g. Fahey et al., 1990; Proffitt et al., 1990; Müller et al., 1996; Esler and Waugh, 2002).

The Stratosphere-TRoposphere Experiments by Aircraft Measurements (STREAM) 1998 campaign was performed in Timmins, Canada (48.2°N, 79.3°W), in July 1998. Details of the campaign as well as results deduced from the measurements can be found elsewhere (Lange et al., 2001; Fischer et al., 2002; Hoor et al., 2002; de Reus et al., 2003; Scheeren et al., 2003). Here, we will show that during the flight on 15 July 1998 dehydration was observed in the tropopause region of the northern hemisphere mid-latitudes. Dehydration, that is, the removal of water vapour from the gas phase, can either be a reversible or an irreversible process depending on the lifetime of water-containing particles and their size. However, it is generally defined as an irreversible process since the particles live long enough to fall and remove

*Corresponding author.
e-mail: f.khosrawi@fz-juelich.de
DOI: 10.1111/j.1600-0889.2006.00182.x

water permanently from an air mass (Schiller et al., 1999, 2002). Dehydration in the stratosphere is generally observed over the Antarctic during winter (e.g. Kelly et al., 1989; Vömel et al., 1995; Nedoluha et al., 2000) and to a lesser extent also over the Arctic (e.g. Fahey et al., 1990; Vömel et al., 1997; Pan et al., 2002; Schiller et al., 2002) and further at the tropical tropopause (e.g. Jensen et al., 1996; Clark et al., 2003; Read et al., 2004). Dehydration in the mid-latitudes has so far only been observed once (Durry et al., 2002). Durry et al. (2004) report a dehydration event that occurred in the lower stratosphere in connection with a tropical filament. In our study, we will present a case where dehydration of a tropospheric air mass was observed in the mid-latitudes in connection with a polar filament. Therefore, such a case is reported here for the first time. The presence of dehydration is strong evidence that ice particle formation with subsequent sedimentation of these particles occurred in these air masses (Schiller et al., 1999, 2002). In order to reach substantial sedimentation rates, ice particles must grow to a radius of at least 10 μm (e.g. Müller and Peter, 1992; Jensen et al., 1996; Nedoluha et al., 2002). Indeed, it has recently been reported (Hallar et al., 2004) that in cold Arctic cirrus a significant fraction of total water is contained in ice particles with $r > 40\,\mu$m.

Since it is generally assumed that the majority of particles in the tropopause region consist of H_2SO_4/H_2O (Brock et al., 1995) and that ice particles are formed by homogeneous freezing of H_2SO_4/H_2O aerosols (e.g. Heymsfield and Miloshevich, 1993; Jensen et al., 1998) it needs to be investigated whether condensation of H_2O on such particles has occurred. However, results derived from recent campaigns show that especially in the polluted northern hemisphere mid-latitudes the heterogeneous ice formation on insoluble particles (ice nuclei) plays an important role (Ovarlez et al., 2002; Haag et al., 2003; Ström et al., 2003). Black carbon (DeMott et al., 1999) and mineral particles (Chen et al., 1998; Petzold et al., 1998; Sassen, 2005) have been suggested, for example, as potential ice nuclei for heterogeneous freezing.

We will identify the dehydration based on measurements of the STREAM 1998 campaign using the relationship between H_2O and O_3. Further, trajectory and box model studies were carried out to address the question whether the air mass has been dehydrated through condensation of H_2O on H_2SO_4/H_2O particles and homogeneous freezing of these particles with subsequent sedimentation. By considering saturation ratios along the trajectories we will examine whether the requirements for homogeneous freezing of H_2SO_4/H_2O aerosol particles are fulfilled. First, we investigate the growth processes of the liquid aerosols since H_2SO_4/H_2O aerosols can exist as supercooled droplets at very low temperatures. Using a box model (Khosrawi and Konopka, 2003) we will simulate the amount of H_2O that condensed onto liquid H_2SO_4/H_2O particles. Additionally, the possibility that heterogeneous freezing is involved in the ice particle formation that caused the dehydration will be discussed.

2. Meteorology and *in situ* observations

2.1. Meteorological analysis

The detailed analysis of meteorological conditions during the STREAM flight on 15 July 1998 was presented earlier (Beuermann et al., 2002) on the basis of potential vorticity (PV) maps on isentropic surfaces interpolated from ECMWF analyses. Therefore, ECMWF analyses on 14 isobaric surfaces with a vertical resolution at the tropopause of 100 hPa and a horizontal resolution of $1^\circ \times 1^\circ$ in longitude and latitude were used. In the PV maps, on the 330 K isentropic surface, a region characterized by stratospheric air was located over the western coast of Canada on 14 July. Originating from this air mass an elongated streamer propagated eastward. At the same time a trough of cold, polar stratospheric air developed and was transported into the mid-latitudes. The two stratospheric air masses were advected to the region of Hudson Bay towards 16 July and spun up cyclonically around each other leading to the formation of an anchor-shaped structure in the vicinity of the polar jet stream (Beuermann et al., 2002).

2.2. In situ observations

Several *in-situ* instruments measuring the trace gas composition (e.g., H_2O, CO, CO_2, CFCs, N_2O, NO, O_3) were on board the Cessna Citation II twin jet aircraft, operated by the University of Delft (Netherlands). The flight on 15 July 1998 (22.30–01.30 UTC) was conducted in dry and almost cloud-free air (Fischer et al., 2002). The outward leg (22:30–00:20 UTC) was at an altitude of 7.8 km (330 K) while the return leg (00:20–01:30 UTC) was at an altitude of 9.8 km (335 K). Fields of equivalent PV obtained by the reverse-domain filling technique and measurements of several trace gases show a pronounced filamentation during the flight (Beuermann et al., 2002).

Here, we focus on the measurements of H_2O, O_3, N_2O and CO. The H_2O data were obtained by the Lyman-α-fluorescence fast *in-situ* stratospheric hygrometer (FISH) measuring total water (Zöger et al., 1999) and the O_3 data by an ozone chemiluminescence monitor (Bregman et al., 1995). Both instruments make measurements with a temporal resolution of one second. The overall accuracy of FISH is 6% and the precision is better than 0.2 ppmv or 3%, while ozone is measured with a precision and accuracy of 5%. Since FISH measures total water, water is measured in the vapour and condensed phase. Further, due to the inlet which is designed for anisokinetic sampling, ice particles are detected sensitively (Schiller et al., 1999). CO and N_2O mixing ratios were determined by using a tunable diode laser absorption spectroscopy (TDLAS) instrument (Fischer et al., 2002). The TRISTAR (Tracer *in-situ* TDLAS for atmospheric research) instrument from the Max Planck Institute for Chemistry allows measurements of up to three trace gases simultaneously with a temporal resolution of 1 s. The measurement precision is $\pm 3.5\%$

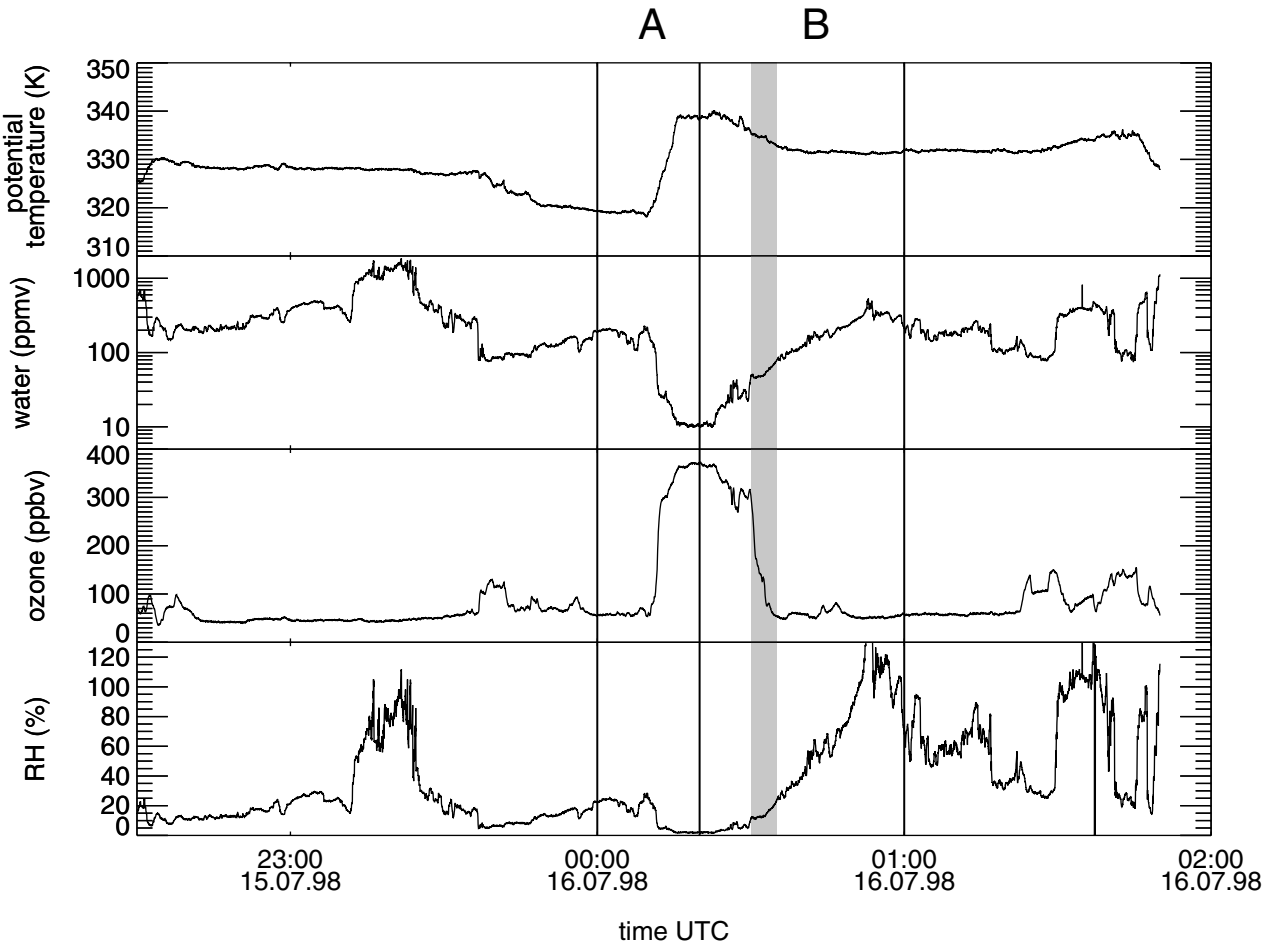

Fig. 1. Measurements of potential temperature, H_2O, O_3 and relative humidity over water on 15 July 1998. The transition from troposphere to stratosphere is marked by part A (00:00–00:20 UTC) and the transition from stratosphere to troposphere is marked by part B (00:20–01:00 UTC). The endpoint of the outward leg coincides with the line marking the transition from part A to part B (00:20 UTC). The grey-coloured area marks the time period when the dehydration has occurred (00:30–00:35 UTC).

for CO and for N_2O at the 1-σ level. On board the Cessna citation measurements were also made with a condensation particle counter (CPC) and an optical particle counter (OPC) measuring the total number of aerosol particles with diameter dp $>$ 6 nm, dp $>$ 18 nm and dp $>$ 120 nm (de Reus et al., 1999).

Potential temperature was derived from the on-board temperature and pressure sensors. The time series of the measurements of potential temperature, water, ozone and relative humidity are shown in Fig. 1. Though the measurements were performed in almost cloud-free air high saturations exceeding 100% are found. These occurences of supersaturated areas in cloud-free air could have been caused by cloud particles that entered the inlet and thus could be an indicator for subvisible cirrus clouds. Time series of H_2O and O_3 show strong variations of mixing ratios during the flight caused by the interception of stratospheric filaments within the tropospheric air. A deep intrusion of stratospheric air was crossed from 00.10–00:35 UTC. In the data this is reflected by high ozone mixing ratios ($\geq$100 ppbv), low water mixing ratios ($\leq$10 ppmv) and low relative humidity values (Fig. 1). However, at the edge of the filament, compared to the O_3 and the other components [e.g. CO and N_2O (not shown)] the water mixing ratios very slowly reach the tropospheric values (00:30–00:35 UTC). This slow recovery of H_2O indicates that water in the tropospheric air mass is missing at the edge of the filament. Because FISH measures total water the missing water cannot be sequestered in ice particles. Thus, condensation of H_2O followed by sedimentation of H_2O-containing particles may have caused the dehydration of the air mass.

3. Tracer–tracer correlations

To identify dehydration, the relationship between O_3 and H_2O is used. For the time interval where the Cessna Citation probed stratospheric air on 15 July, the measurements of H_2O and O_3 were temporally separated in the transition between troposphere to stratosphere (00.00–00.20 UTC, part A in

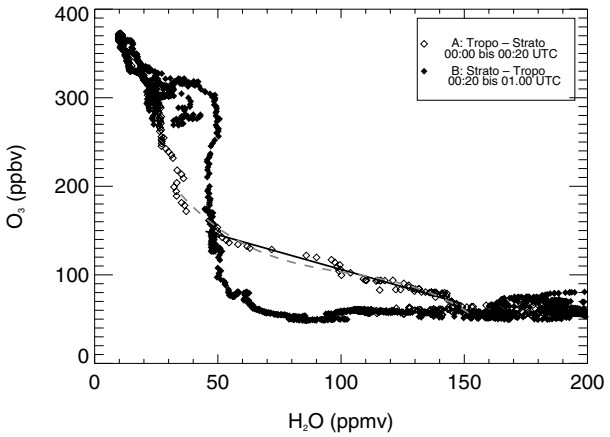

Fig. 2. Correlation of H_2O and O_3 for the flight on 15 July for the time interval from 00:00 to 01:00 UTC divided into two parts: transition from troposphere to stratosphere (00:00–00:20 UTC) and transition from stratosphere back to troposphere (00:20–01:00 UTC). Additionally shown is the linear fit (solid line, eq. 1) and the polynomial fit (dashed line, eq. 1) through the mixing layer valid for $45 < H_2O < 150$ ppmv and $35 < H_2O < 155$ ppmv, respectively.

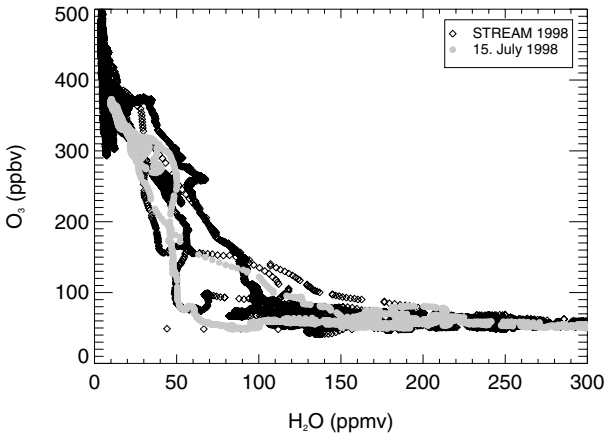

Fig. 3. H_2O/O_3 correlation of STREAM 1998 flight on 15 July (grey bullets) and two other flights (3 July and 8 July) of the STREAM 1998 campaign (black diamonds).

Fig. 1) and stratosphere to troposphere (00.20–01.00 UTC, part B in Fig. 1).

If mixing processes across the subtropical tropopause are neglected, the resulting idealized relation of H_2O and O_3 will display a steep transition between stratospheric and tropospheric air masses (Hoor et al., 2002). However, an exchange between troposphere and stratosphere generally exists and, through the mixing of air masses, leads to the formation of a mixing layer at the interface between tropospheric and stratospheric air. The correlation for the transition between troposphere and stratosphere on 15 July shows the typical pattern for a mixing layer (Hoor et al., 2002; Krebsbach et al., 2005). The correlation of the transition between stratosphere and troposphere, in contrast, shows a steep transition (50–300 ppbv O_3), which would result if tropospheric and stratospheric air masses were exactly separated (Fig. 2, filled symbols). If stratospheric and tropospheric air masses are exactly separated the correlation would have a L-shape, with the stratospheric values on the *y*-axis and the tropospheric values on the *x*-axis (Hoor et al., 2002). Thus, the measured water concentrations indicate that the air mass has been dehydrated since the intensity of mixing must have been low and a mixing line is definitely not found for the transition from stratosphere to troposphere. The O_3/H_2O correlation for the transition from the stratosphere to troposphere (return leg) closely resembles an 'L-shape' relation. Any mixing that could have occurred would have smoothed the O_3/H_2O correlation. Thus, mixing can clearly be excluded as the cause of the anomalously low H_2O mixing ratios. Between 180 and 320 ppbv O_3 the correlation also shows an area with enhanced water vapour mixing ratios which, however, lies in the range of variability as discussed by Krebsbach et al. (2005) and as can be seen in comparison with the correlations of two other flights (3 July and 8 July 1998) of the STREAM 1998 campaign (Fig. 3).

The H_2O values for the flight on 15 July are much lower for the transition from stratosphere to troposphere (Fig. 2) than for the transition from troposphere to stratosphere (Fig. 2). At 80 ppbv O_3, around 150 ppmv H_2O was found during the transition from troposphere to stratosphere while during the transition from stratosphere to troposphere only 80 ppmv H_2O was measured. That the measured H_2O values are very low can also be seen in the comparison of the correlation of the flight of 15 July with the correlations of two other flights (3 July and 8 July 1998) of the STREAM 1998 campaign (Fig. 3). Much lower water mixing ratios were found at ozone mixing ratios between 50 and 70 ppbv for the flight on 15 July. For the two other flights at 50 ppbv ozone a water mixing ratio of around 100 ppmv was found while for the flight on 15 July only 70 ppmv was found. The STREAM 1998 campaign was carried out in mid-latitudes, and using trajectory analysis the air masses during this campaign have been identified as of polar and mid-latitude origin (Fischer et al., 2002).

Tracer–tracer correlations of N_2O and CO and of CO and O_3 (Fig. 4) further corroborate that the shape of the correlation for the return leg (transition stratosphere to troposphere) in the correlation of H_2O and O_3 cannot be caused by mixing. The correlation between N_2O and CO as well as the correlation between CO and O_3 cover the same range of H_2O mixing ratios and only small differences between the correlation of the outward and return leg are noticeable. Further, the possibility that the missing water in the return leg of the correlation of H_2O and O_3 was incorporated in particles can be excluded since FISH measures total water, that is, condensed and vapour phase (Schiller et al., 1999). Hence, if water-containing particles were present in the sampled air masses they would have been clearly detected by FISH. Therefore, H_2O in the particle phase can be excluded as the cause of the anomaly in the correlation of the return leg.

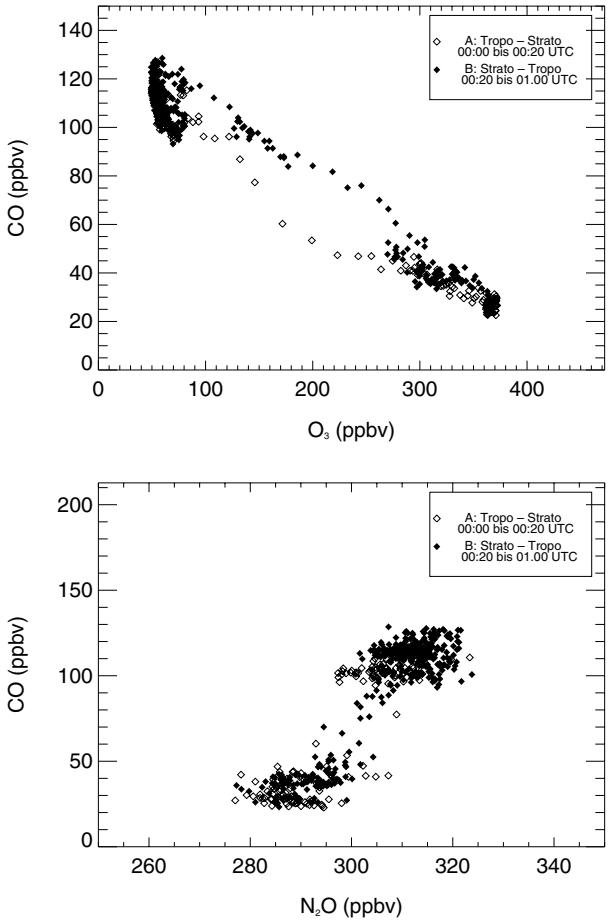

Fig. 4. Correlation of CO and O_3 (top) and N_2O and CO (bottom) for the time interval from 00:00 to 01:00 UTC divided into two parts: transition from troposphere to stratosphere (00:00–00:20 UTC) and transition from stratosphere back to troposphere (00:20–01:00 UTC).

The amount of water that was present in the atmosphere before the air mass was dehydrated is estimated by using the correlation of the outward leg (the transition between troposphere and stratosphere) as a reference (Fig. 2). Thus, by using the O_3 mixing ratio measured during the return leg and the correlation derived for the outward leg an estimate for the undehydrated water mixing ratio can be given. The mixing of stratospheric and tropospheric air generally result in linear mixing lines (Hoor et al., 2002). Thus, to estimate the undehydrated water mixing ratios from the correlation of the outward leg a linear fit of the data along the mixing line (H_2O between 45 and 150 ppmv and 00:10 to 00:20 UTC) was calculated. The linear fit yields

$$O_3 = 184.41 - 0.78 * H_2O, \tag{1}$$

with O_3 in ppbv and H_2O in ppmv. From eq. (1) the undehydrated water mixing ratio H_2O^* can be calculated as:

$$H_2O^* = \frac{O_3 - 184.41}{-0.78}. \tag{2}$$

Table 1. Measured and estimated mixing ratios and maximum relative humidity derived along the selected trajectories. H_2O and O_3 are the concentrations measured at the given times during the return leg. H_2O^* denotes the undehydrated water mixing ratio estimated from the outward leg (see text for further details) and ΔH_2O the difference between measured and the undehydrated water mixing ratios. RH_w and RH_i are the maxima of the saturation ratios over water and ice derived with H_2O^* and the minimum temperature T_{min} along the selected trajectories

Traj	Time UTC	H_2O ppmv	O_3 ppbv	H_2O^* ppmv	ΔH_2O ppmv	RH_w %	RH_i %	T_{min} K
A	00:32:00	47.7	139.8	58.0	10.3	35	62	218
B	00:32:40	50.4	101.9	103.0	52.6	63	112	218
C	00:33:00	55.1	78.6	137.0	81.9	85	148	218
D	00:34:00	63.1	65.3	147.0	89.9	93	162	218
E	00:35:00	76.1	55.0	153.0	76.9	97	170	218

However, in this study we use a polynomial fit, which covers a larger part of the correlation than the mixing line alone. This is appropriate here since the ozone measurements of the trajectories starting at 00:34 and 00.35 UTC give lower values than 70 ppbv O_3, thus leading to H_2O^* values not covered by the validity range of the linear fit. However, as a reference for the mixing line in any case the linear fit should be used. The polynomial fit used in this special case yields (H_2O between 35 and 155 ppmv and 00:10 to 00:20 UTC)

$$O_3 = 352.87 - 6.45 * H_2O + 5.86 * 10^{-2} * H_2O^2 - 1.91 * 10^{-4} * H_2O^3, \tag{3}$$

with O_3 in ppbv and H_2O in ppmv. The curve resulting from this undehydrated water mixing ratio H_2O^* (Table 1) derived with the linear fit is shown in Fig. 5 (dotted line).

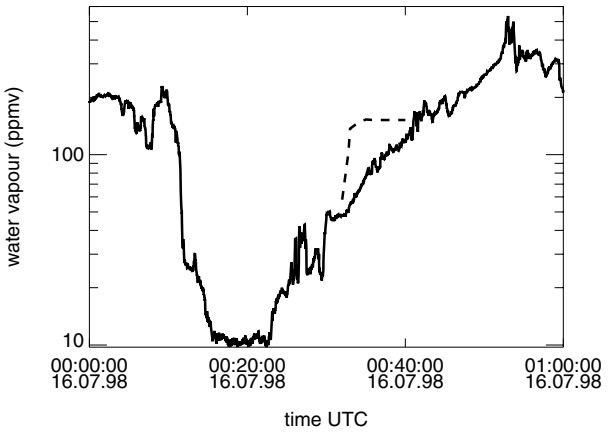

Fig. 5. Water measurements on 16 July 1998 between 00:00 and 01:00 UTC (solid line). The dotted line represents the corrected curve for water derived by the estimating the undehydrated water mixing ratio H_2O^* (00:30–00:35 UTC).

4. Trajectory and box model studies

4.1. Ice saturation

Isentropic trajectories based on ECMWF analyses with a temporal resolution of $\Delta t = 6$ hr were calculated backwards for 10 d starting at each point of the measurements for the flight on 15 July ($\Delta t = 1$ s). Between 00:15 and 00:45 UTC all trajectories show the same characteristic. During this time interval a strong but slow temperature decrease followed by a warming is found a few days before the flight as already pointed out by Khosrawi and Konopka (2003). From the ozone measurements, the time interval when the water mixing ratios should reach the tropospheric values is estimated as being between 00:30 and 00:35 UTC. Trajectories starting during this time interval were selected for investigating whether saturation ratios over ice were reached that are sufficient for homogeneous freezing of H_2SO_4/H_2O particles (Table 1).

Since the measurements have a temporal resolution of $\Delta t =$ 1 s, and trajectories were calculated for each point of the measurements, 60 trajectories per minute are obtained. To simplify matters, between 00:30 and 00:35 UTC the first trajectory every minute was selected since during this short time interval differences between the trajectories are expected to be small. The trajectories at 00:30 and 00:31 UTC were not used for the ice saturation studies since these were in the area where enhanced water mixing ratios were measured (which however lie in the range of variability as discussed above; values between 30 and 50 ppmv H_2O and 150 and 320 ppbv O_3 in Fig. 2). A second trajectory was chosen at 00:32 UTC (00:32:40 UTC) in order to have one trajectory in our study that has a mean O_3 mixing ratio around 100 ppbv, thus, a mixing ratio that lies between the O_3 mixing ratio of the trajectory starting at 00:32 UTC (139.8 ppbv) and the trajectory starting at 00:33 (78.6 ppbv). Thus, the selected trajectories start between 00:32 and 00:35 UTC.

The threshold value for the supersaturation required for homogeneous nucleation is a function of temperature (Koop et al., 2000). For the homogeneous formation of ice particles a saturation ratio of 80% over water is required (Jensen et al., 1994), and 130–150% over ice at temperatures of T < 240 K (Tabazadeh et al., 1997a; Koop et al., 2000). Using the undehydrated water mixing ratio H_2O^* the saturation ratios over ice and water, respectively, were calculated for the selected trajectories. The differences ΔH_2O between the undehydrated and measured water mixing ratios H_2O^* and H_2O, respectively, are 10.3 ppmv (00:32 UTC), 52.6 ppmv (00:33 UTC), 81.9 ppmv (00:33 UTC), 89.9 ppmv (00:34 UTC) and 76.9 ppmv (00:35 UTC) as listed in Table 1. While both trajectories starting at 00:32 UTC reached only very low saturations, the trajectories between 00:33 and 00:35 UTC reached the supersaturation required for ice formation through homogeneous freezing (Table 1, maximum saturations of 85%, 93%, 97% over water and 148%, 162%, 170% over ice, respectively). The temperature along these trajectories

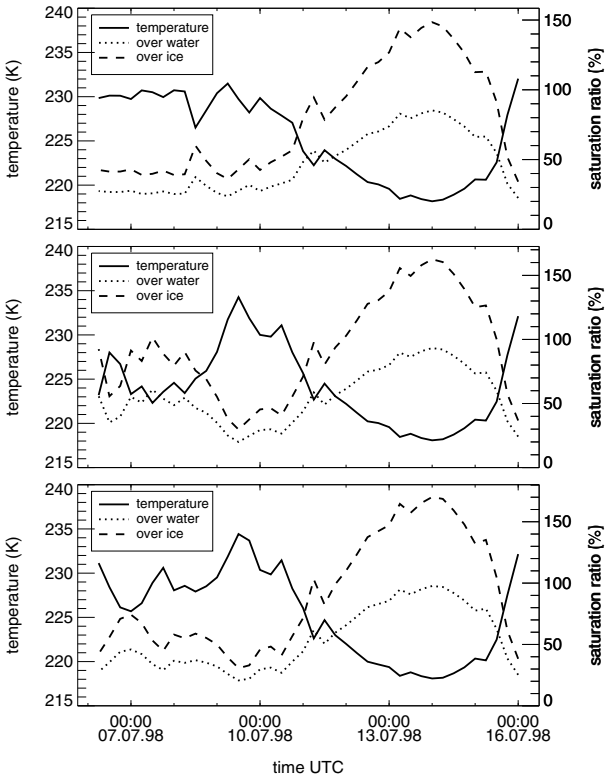

Fig. 6. Temperature and saturation ratios over water and ice along the selected trajectory (top: Traj = C, $H_2O^* = 137$ ppm, middle: Traj = D, $H_2O^* = 147$ ppm, and bottom: Traj = E, $H_2O^* = 153$ ppm).

and the corresponding saturation ratios over water and ice are shown in Fig. 6. Between 6 and 9 July along the trajectories a different temporal temperature development is found. However, on 9 July the temperature along all these three trajectories starts to decrease very strongly, but at a slow cooling rate, until 14 July by about 16 K from about 234 K to 218 K (cooling rate of ≈0.17 K/hr). After reaching the minimum temperature, when also the highest saturation ratios are reached, the temperatures begin to increase and approach about 232 K and ice saturation ratios of ≈35% on 16 July between 00:33 and 00:35 UTC, at the times of the measurements.

4.2. Condensation processes

In the following, we will discuss whether the sulphuric acid aerosol particles can grow by the uptake of the available H_2O so that these particles become diluted enough to freeze homogeneously and subsequently sediment out. Studies by Koop et al. (2000) have shown that the homogeneous ice formation from supercooled aqueous solutions is independent of the nature of the solute, but depends only on the water activity, and thus the dilution, of the solution. The most fundamental requirement for the dehydration of an air mass due to sedimentation is that the ice

particles must grow large enough to fall a significant distance. Model studies have shown that for efficient dehydration ice particles must grow to a size of at least 10 μm in radius (e.g. Müller and Peter, 1992; Jensen et al., 1996; Nedoluha et al., 2002). Further, model studies have shown that the largest particles freeze first (e.g. Jensen and Toon, 1994; Tabazadeh et al., 1997b). However, this has so far not been confirmed by measurements in the atmosphere.

Here, we use a box model to study the growth of sulphuric acid aerosols for conditions on 15 July. The box model simulates the condensation of HNO_3 and H_2O on the liquid H_2SO_4/H_2O aerosol particle using the parametrization of Luo et al. (1995) for the partial pressures of HNO_3 and H_2O. The box model is initialized with a log-normal distributed particle ensemble of pure H_2SO_4/H_2O aerosol particles. The distribution is divided into 25 size bins with a volume ratio of 2, starting at a minimum particle radius of 1 nm. For the log-normal distribution the following parameters, representing an upper tropospheric aerosol distribution, are used: total number of particles $n = 10^3$ cm^{-3} [from the CPC measurements (de Reus et al., 1999) on 15 July 1998], width of $\sigma = 1.8$ and mean radius $r_m = 0.08$ μm. For each size bin, the time evolution is calculated along the trajectories considering condensation processes. A short description of the model can be found in Khosrawi and Konopka (2003) and a more detailed one in Khosrawi (2001). Uncertainties of the water measurements and temperature variations due to gravity waves were not considered in the box model simulations. However, the influence of these uncertainties on ice saturation and thus, on the freezing process, will be discussed in Section 4.4.

The box model simulations were performed for the trajectories starting at 00:33, 00:34 and 00:35 using the undehydrated water mixing ratios H_2O^* calculated from the ozone measurements (Table 1). However, the box model simulations along the selected trajectories show no significant condensation (Figs. 7–9). Some uptake of HNO_3 occurs resulting in 5–10wt% of HNO_3 in the particles. Somewhat larger amounts of H_2O condense on the particles increasing the mass fraction of H_2O from 50wt% to 80wt% to 95wt%. However, both the H_2O and HNO_3 uptake leads to a growth of the particles which is not sufficient for freezing (e.g. 0.1–0.3 μm for the trajectory starting at 00:35 UTC). Further, with increasing H_2O and HNO_3 in the particles the amount of H_2SO_4 in the particles is strongly reduced (down to 5–10wt%).

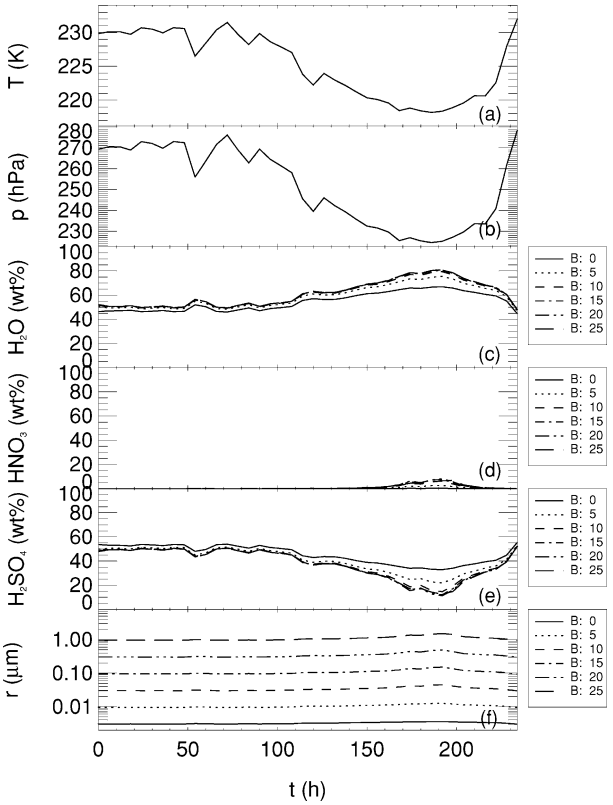

Fig. 7. Modelled change of H_2SO_4/H_2O particle ensemble due to condensation (Traj = C, $H_2O^* = 137$ ppm): (a) temperature, (b) pressure, (c) mass fraction of H_2O, (d) mass fraction of HNO_3, (e) mass fraction of H_2SO_4 and (f) radius of the particle of bin size B0–B25. B0 marks the smallest and B25 the largest bin size.

4.3. *Ice formation processes*

Homogeneous freezing of binary H_2SO_4/H_2O aerosol particles requires substantial ice supersaturations. Similar arguments hold for liquid ternary $H_2SO_4/H_2O/HNO_3$ aerosols (Chen et al., 1999; Petzold et al., 2000). Since in our trajectories a minimum temperature of 218 K was reached saturation ratios of about 150% are required for the homogeneous freezing of H_2SO_4/H_2O particles (Koop et al., 2000). Such high saturation ratios were reached along the trajectories starting at 00:34 and 00:35 UTC on 14 July at around 00:00 UTC. Besides the minimum temperature and maximum saturation ratio reached also the time interval during these conditions prevail is of importance for the freezing process. The saturation ratios remain for both trajectories above 150% until 15 July 12:00 UTC (Fig. 6). Thus, a time interval of around 36 hr results where the particles could have potentially grown, frozen homogenously and sedimented out.

Saturation ratios of about 130%, which are required for heterogeneous freezing, are reached much earlier, namely on 13 July at around 00:00 UTC. Therefore, the time interval where heterogeneous freezing could have occurred is longer at around 72 hr. Consequently, the particles have twice as much time to freeze heterogeneously than homogeneously. Further, the conditions for heterogeneous freezing were reached 24 hr earlier than for homogeneous freezing. Additionally, if the particles start to freeze heterogeneously the supersaturations will decrease so that saturation ratios required for homogeneous freezing may probably no longer be reached after heterogeneous freezing has started. However, the heterogeneous freezing process is not only

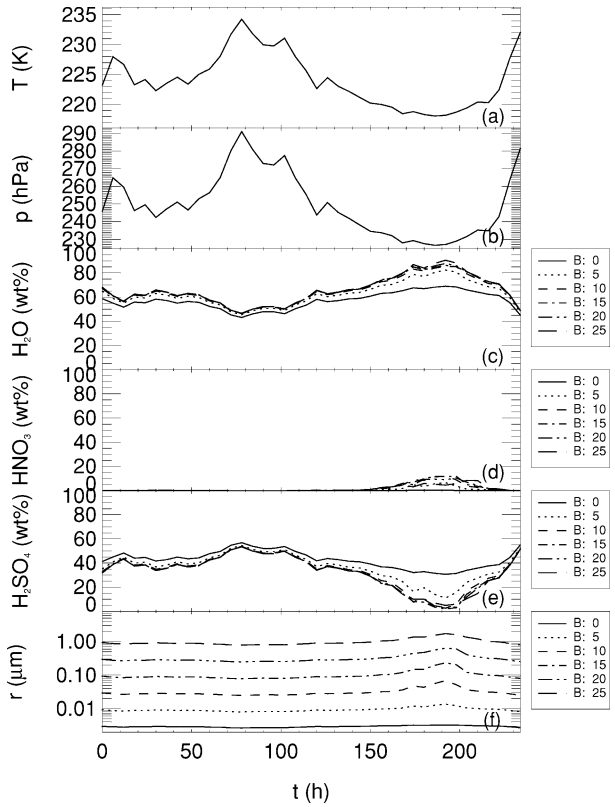

Fig. 8. Modelled change of H_2SO_4/H_2O particle ensemble due to condensation (Traj = D, $H_2O^* = 147$ ppm): (a) temperature, (b) pressure, (c) mass fraction of H_2O, (d) mass fraction of HNO_3, (e) mass fraction of H_2SO_4 and (f) radius of the particle of bin size B0–B25. B0 marks the smallest and B25 the largest bin size.

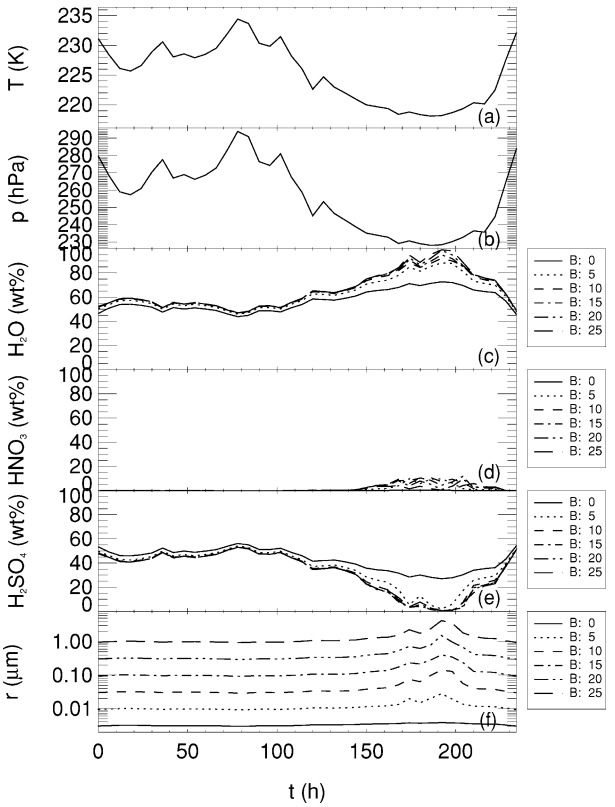

Fig. 9. Modelled change of H_2SO_4/H_2O particle ensemble due to condensation (Traj = E, $H_2O^* = 153$ ppm): (a) temperature, (b) pressure, (c) mass fraction of H_2O, (d) mass fraction of HNO_3, (e) mass fraction of H_2SO_4 and (f) radius of the particle of bin size B0–B25. B0 marks the smallest and B25 the largest bin size.

dependent on the nature of the ice nuclei and the freezing humidity but also on the number of ice nuclei present. A high number of ice nuclei present enhances the probability of heterogeneous nucleation to occur. High numbers of ice nuclei are especially found in polluted regions and results from recent campaigns have shown that in such regions the heterogeneous freezing of insoluble particles plays an important role (Ovarlez et al., 2002; Haag et al., 2003; Ström et al., 2003). Measurements of ice nuclei were not made during STREAM 1998, thus, making it difficult to estimate the influence of heterogeneous freezing on the observed dehydration.

A rough estimate of the number of ice particles which could have been formed homogeneously (if we consider this as the only freezing process) can be derived from the results of Kärcher and Lohmann (2002). If besides homogeneous nucleation also heterogeneous nucleation has occurred the number of homogeneously nucleated particles should be rather lower. The results by Kärcher and Lohmann (2002), derived from numerical simulations, give the relationship between ice particle number densities and vertical velocities. Since our cooling event was caused by slow vertical motions (synoptic motions) with low cooling rates of 0.17 K hr^{-1} a low ice particle number density of less than 10^{-1} cm^{-3} based on homogeneous nucleation theory can be expected.

Further, recent studies (e.g. Kärcher and Ström, 2003; Haag and Kärcher, 2004)have shown that subgrid scale variability which is not resolved by the ECMWF analyses, can significantly enhance homogeneous ice particle formation. The vertical updrafts can be much faster than given by the ECMWF model. We performed box model simulations with superimposed fluctuations on the synoptic temperatures (random amplitudes up to 2 K and a mean period of 1200 s) and obtained the same results as presented in Figs. 7–9 using synoptic temperatures (not shown). Further, the synoptic cooling rates for the conditions on 15 July 1998 investigated here are much lower than the synoptic cooling rates considered in the studies by Kärcher and Ström (2003) and Haag and Kärcher (2004). Thus, it seems that subgrid scale variability has no influence on our results. Further, as reported by DeMott et al. (1997) and Gierens (2003), heterogeneous ice formation becomes an important ice formation process in cases of slow gradual cooling of air as is the case here.

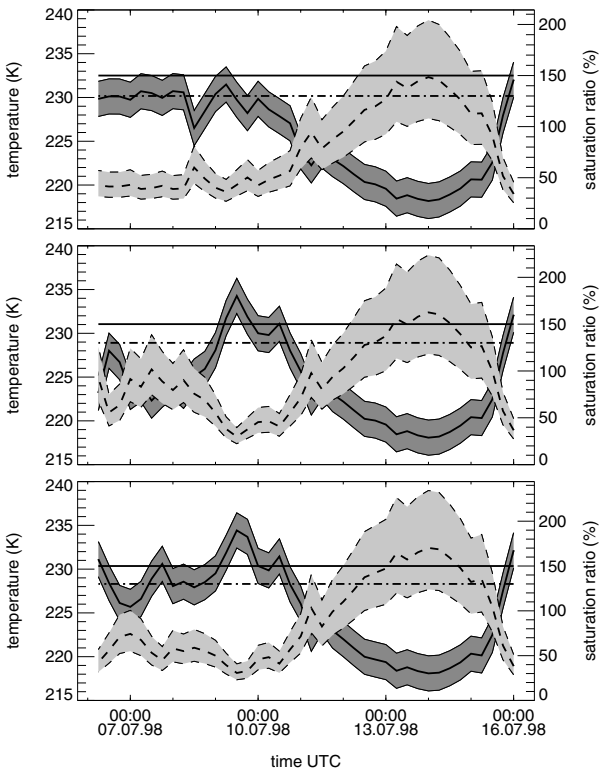

Fig. 10. Variation of the calculated ice saturation ratios considering the uncertainty in the water measurements by FISH (±6%) and variation in the temperatures caused by gravity waves (±2 K). Top: Traj = C, middle: Traj = D, bottom: Traj = E. Dark grey: temperature, light grey: ice saturation, solid line: threshold ice saturation for homogeneous nucleation, dashed line: threshold ice saturation for heterogeneous nucleation.

4.4. Impact of temperature variation and water uncertainty

Here, we will investigate how a variation in temperature of ±2 K due to gravity waves and the uncertainty of ±6% in the measurements of total water will influence the ice saturation ratios reached along the trajectories started between 00:33 and 00:35 UTC. Therefore, we recalculated the ice saturation ratios shown in Fig. 6 using these uncertainties. The results of this sensitivity study are shown in Fig. 10. If we assume colder temperatures and a higher water mixing ratio, very high supersaturations of 200%, 220% and 230% over ice could be reached in the absence of ice formation and growth. In all three trajectories the saturation ratio exceeds the threshold level for heterogeneous and homogeneous nucleation and these conditions prevail for about 3–4 d (72–96 hr). The onset for homogeneous nucleation is exceeded 12 hr later than the onset level for heterogeneous freezing, thus, much earlier than in our case described in the previous section. However, if we assume higher temperatures and a lower water mixing ratio, quite low saturation ratios (105%, 115% and 120% over ice) are reached and in all trajectories neither the saturation ratios required for homogeneous freezing nor for heterogeneous freezing are reached. This sensitivity study again shows how difficult it is to determine which process, heterogeneous or homogeneous freezing, was responsible for the ice formation. This again states, that most probably both processes were involved in the freezing process. Thus, most likely, a combination of homogeneous and heterogeneous freezing was involved in the ice particle formation with subsequent sedimentation that caused the dehydration observed on 15 July.

5. Discussion

For the flight on 15 July 1998 which was performed in the vicinity of the polar jet stream over Canada, both RDF calculations and observations show an intrusion of stratospheric air penetrating deep into the troposphere (Beuermann et al., 2002). Time-series of the measurements show that along the flight path H_2O reaches the tropospheric values very slowly at the edge of the filament compared to the other components. Correlations of O_3 and H_2O, which were separated into the transition from stratosphere to troposphere and troposphere to stratosphere, provide evidence of dehydration since for a certain O_3 mixing ratio in the latter transition much lower H_2O mixing ratios were found than in the former transition. Thus we conclude that ice particle formation with subsequent sedimentation of these particles dehydrated the air mass.

Box model studies were carried out to address the question of the composition of the aerosol particles that dehydrated the air mass. The majority of aerosol particles in the tropopause region consist of H_2SO_4/H_2O and it is generally assumed that homogeneous freezing of these particles is the main freezing process (Heymsfield and Miloshevich, 1993; Jensen et al., 1998). Thus, we investigated whether condensation of H_2O on H_2SO_4/H_2O particles and freezing of these particles with subsequent sedimentation could be responsible for the observed dehydration on 15 July 1998. However, our results show no significant growth of H_2SO_4/H_2O particles due to water uptake.

Measurements by Ström and Ohlsson (1998) show that in regions with heavy air traffic ice particles often contained some absorbing material (probably soot), and moreover such inclusions were most frequent at those altitudes where air traffic routes are concentrated (8–12 km). In fact, the air measured on 15 July was polluted as shown by Fischer et al. (2002) on the basis of CO measurements. In addition, measurements support the hypothesis that ice particle formation occurs both by heterogeneous nucleation by insoluble particles and homogeneous freezing of particles containing solutions (DeMott et al., 2003; Haag et al., 2003). Most heterogeneous ice nuclei were identified as relatively pure mineral dusts and metallic particles (DeMott et al., 2003; Cziczo et al., 2004). However, no measurements of ice nuclei were made during the STREAM 1998 campaign, thus, making it difficult to give a reliable statement on the role that

heterogeneous ice formation played for the observed dehydration on 15 July.

6. Conclusion

In our study an observation of dehydration in the mid-latitude upper troposphere has been presented for the first time. This dehydration was caused by sedimentation of ice particles. Using the uncertainty of the water measurements and the variation of temperature due to gravity waves, it is not possible to determine which freezing process, homogeneous or heterogeneous, was responsible for the dehydration of the air. Both heterogeneous and homogeneous freezing thresholds were reached along the trajectories. Taking into account the location of the measurements, which were performed in the polluted northern hemisphere, together with the results derived from recent measurements (Ström et al., 2003; Haag et al., 2003; Haag and Kärcher, 2004) and the slow vertical motion by the trajectories suggest that both heterogeneous and homogeneous nucleation could have been involved in the freezing process. Thus, our study supports the hypothesis that especially in this region ice particles are not regularly formed solely by homogeneous freezing of H_2SO_4/H_2O aerosols. Other components (e.g. carbon, soot, minerals) as measured by Murphy et al. (1998), Chen et al. (1998) and Cziczo et al. (2004), which can induce the heterogeneous ice formation process should be taken into account in future ice formation studies.

7. Acknowledgments

We would like to thank P. Deuflhard and U. Nowak for providing the solver for the ordinary differential equations used in the box model. We also would like to thank J. Lelieveld for the ozone data, H. Fischer for the nitrous oxide and carbon monoxide data, J. Ström for the aerosol data and B. Kärcher, M. Krämer and A. Mangold for helpful discussions. We thank both the anonymous reviewers for their helpful comments. We also thank J. Carter-Sigglow for revising the grammar and style of the manuscript. This work was supported by the BMBF in the AFS project under grant 07 AF 205 and by the EC 5th Framework Project PARTS (EKV2-2001-00051).

References

Beuermann, J., Konopka, P., Brunner, D., Bujok, O., Günther, G. and co-authors. 2002. High-resolution measurements and simulation of stratospheric and tropospheric intrusions in the vicinity of the polar jet stream. *Geophys. Res. Lett.* **29**, doi: 10.1029/2001GL014162.

Bregman, A., Velthoven, van, P. F.J., Wienhold, F. G., Fischer, H., Zenker, T. and co-authors. 1995. Aircraft measurements of O_3, HNO_3, and N_2O in the winter Arctic lower stratosphere during the Stratosphere-Troposphere Experiment by Aircraft Measurements (STREAM) 1. *J. Geophys. Res.* **100**, 11 245–11 260.

Brock, C. A., Hamill, P., Wilson, J. C., Jonsson, H. H. and Chan, K. R. 1995. Particle formation in the upper tropical troposphere: A source of nuclei for the stratospheric aerosol. *Science* **270**, 1650–1653.

Chen, Y., Kreidenweiss, S. M., McInnes, L. M., Rogers, D. and DeMott, P. 1998. Single particle analysis of nucleating aerosols in the upper troposphere and lower stratosphere. *Geophys. Res. Lett.* **25**, 1391–1394.

Chen, M., Rood, R. B. and Read, W. G. 1999. Seasonal variations of upper tropospheric water vapor and high clouds observed from satellites. *J. Geophys. Res.* **104**, 6193–6197.

Clark, H. L., Harwood, R. S., Billingham, A. and Pumphrey, H. C. 2003. Cirrus and water vapor in the tropical tropopause layer observed by Upper Atmospheric Research Satellite (UARS). *J. Geophys. Res.* **108**, 4751, doi:10.1029/2003JD003748.

Cziczo, D. J., Murphy, D. M., Hudson, P. K. and Thomson, D. S. 2004. Single particle measurements of the chemical composition of cirrus ice residue during CRYSTAL-FACE. *J. Geophys. Res.* **109**, doi:10.1029/2003JD0004032.

Danielsen, E. F. 1968. Stratospheric-tropospheric exchange based on radioactivity, ozone and potential vorticity. *J. Atmos. Sci.* **25**, 502–518.

de Reus, M., Ström, J., Hoor, P., Lelieveld, J. and Schiller, C., 1999. Particle production in the lowermost stratosphere by convective lifting of the tropopause *J. Geophys. Res.* **104**, 23 935–23 940.

de Reus, M., Fischer, H., Arnold, F., de Gouw, J., Warneke, C. and co-authors. 2003. On the relationship between acetone and carbon monoxide in different air masses. *Atmos. Chem. Phys.* **3**, 1709–1723.

DeMott, P. J., Rogers, D. C. and Kreidenweiss, S. M. 1997. The susceptibility of ice formation in upper tropospheric clouds to insoluble aerosol components. *J. Geophys. Res.* **102**, 19 575–19 854.

DeMott, P. J., Chen, Y., Kreidenweiss, S. M., Rogers, D. C. and Sherman, D. 1999. Ice formation by black carbon particles. *Geophys. Res. Lett.* **26**, 2429–2432.

DeMott, P. J., Cziczo, D. J., Prennni, A. J., Murphy, D. M., Kreidenweiss, S. M. and co-authors. 2003. Measurements of the concentration and composition of nuclei for cirrus formation. *Proc. Natl. Acad. Sci.* **100**, 14 655–14 660.

Durry and co-authors. 2002. In situ measurements of H_2O and CH_4 with Telecommunication Laser Diodes in the Lower Stratosphere: Dehydration and indication of a Tropical Air Intrusion at mid-latitudes. *J. Atmos. Chem.* **13**, 175–194.

Esler, J. G., and Waugh, D. 2002. A method for estimating the extent of denitrification of arctic polar vortex air from tracer–tracer scatter plots. *J. Geophys. Res.* **107**, doi:10.1029/2001JD001071.

Fahey, D. W., Kelly, K. K., Kawa, S. R., Tuck, A. F., Loewenstein, M. and co-authors. 1990. Observations of denitrification and dehydration in the winter polar stratosphere. *Nature* **344**, 321–324.

Fischer, H., Brunner, D., Harris, G. W., Hoor, P., McKenna, D. S. and co-authors. 2002. Synoptic tracer gradients in the upper troposphere over central Canada during the Stratosphere-Ttroposphere Experiments by Aircraft Measurements 1998 summer campaign. *J. Geophys. Res.* **107**, doi:10.1029/2001JD000312.

Gierens, K. 2003. On the transition between heterogeneous and homogeneous freezing. *Atmos. Chem. Phys.* **3**, 437–446.

Haag, W., Kärcher, B., Ström, J., Minikin, A., Lohmann, U. and co-authors. 2003. Freezing thresholds and cirrus cloud formation mechanisms inferred from in situ measurements on relative humidity. *Atmos. Chem. Phys.* **3**, 1791–1806.

Haag, W. and Kärcher, B. 2004. The impact of aerosol and gravity waves on cirrus clouds at mid-latitudes. *J. Geophys. Res.* **109**, D12202, doi:10.1029/2004JD004579.

Hallar, A. G., Avallone, L. M., Herman, R. L., Anderson, B. E. and Heymsfield, A. J. 2004. Measurement of ice water content in tropopause region Arctic cirrus during the SAGE III Ozone Loss and Validation Experiment (SOLVE). *J. Geophys. Res.* **109**, D17203, doi:10.1029/2003JD004348.

Heymsfield, A. J. and Miloshevich, L. M. 1993. Homogeneous ice nucleation and supercooled liquid water in orographic wave clouds. *J. Atmos. Sci.* **50**, 1363–1366.

Holton, J. R., Haynes, P., McIntyre, M. E., Douglass, A. R., Rood, R. B. and Pfister, L. 1995. Stratosphere-troposphere exchange. *Rev. of Geophys.* **33**, 403–439.

Hoor, P., Fischer, H., Lange, L. and Lelieveld, J. 2002. Seasonal variations of a mixing layer in the lowermost stratosphere as identified by the CO-O_3 correlation from in situ measurements. *J. Geophys. Res.* **107**, doi:10.1029/2000JD000289.

Hoskins, B. J. 1991. Towards a PV-Θ view of the general circulation. *Tellus* **43A-B**, 27–35.

Jensen, E. J. and Toon, O. B. 1994. Ice nucleation in the upper troposphere: Sensitivity to aerosol number density, temperature and cooling rate. *Geophys. Res. Lett* **21**, 2019–2033.

Jensen, E. J., Toon, O. B., Westphal, D. L., Kinne, S. and Heymsfield, A. J. 1994. Microphysical modeling of cirrus. 1. Comparison with 1986 FIRE IFO measurements. *J. Geophys. Res* **99**, 10 421–10 442.

Jensen, E. J., Toon, O. B., Pfister, L. and Selkirk, H. B. 1996. Dehydration of the upper troposphere and lower stratosphere by subvisible cirrus clouds near the tropical tropopause. *J. Geophys. Res* **23**, 825–828.

Jensen, E. J., Toon, O. B., Tabazadeh, A., Sachse, G. W., Anderson, B. E. and co-authors. 1998. Ice nucleation processes in upper tropospheric wave-clouds observed during SUCCESS. *Geophys. Res. Lett.* **25**, 1363–1366.

Kärcher, B. and Lohmann, U. 2002. A parameterization of cirrus cloud formation: homogeneous freezing including effects of aerosol size. *J. Geophys. Res.* **107**, doi:10.1029/2001JD001429.

Kärcher, B. and Ström, J. 2003. The roles of dynamical variability and aerosol on cirrus cloud formation. *Atmos. Chem. Phys.* **3**, 823–838.

Kelly, K. K., Tuck, A. F., Murphy, D. M., Proffitt, M. H., Fahey, D. W. and co-authors. 1989. Dehydration in the lower Antarctic stratosphere during late winter and early spring, 1987. *J. Geophys. Res.* **94**, 11 317–11 357.

Khosrawi, F. and Konopka, P. 2003. Enhancement of nucleation and condensation rates due to mixing processes in the tropopause region. *Atmos. Environ.* **37**, 903–910.

Khosrawi, F. 2001. Modellierung der Bildung und des Wachstums von H_2SO_4/H_2O Aerosolen in der Stratosphäre und oberen Troposphäre. *Ph. D. thesis*, Universität Bonn.

Koop, T., Luo, B., Tsias, A. and Peter, T. 2000. Water activity as the determinant for homogeneous ice nucleation in aqueous solutions. *Nature* **406**, 611–614.

Krebsbach, M., Schiller, C., Brunner, D., Günther, G., Hegglin, M. I. and co-authors. 2006. Seasonal cycles and variability O_3 and H_2O in the UT/LMS during SPURT. *Atmos. Chem. Phys.* **6**, 109–125.

Lange, L., Hoor, P., Helas, G., Fischer, H., Brunner, D. and co-authors. 2001. Detection of lightning-produced NO in the mid-latitude upper troposphere during STREAM 1998. *J. Geophys. Res.* **106**, 27 777–27 785.

Luo, B., Carslaw, K. S., Peter, T. and Clegg, S. L. 1995. Vapour pressures of $H_2SO_4/HNO_3/HCl/HBr/H_2O$ solutions to low stratospheric temperatures. *Geophys. Res. Lett.* **22**, 247–250.

Müller, R. and Peter, T. 1992. The numerical modelling of sedimentation of polar stratospheric cloud particles. *Ber. Bunsen-Ges. Phys. Chem.* **96**, 353–361.

Müller, R., Crutzen, P. J., Grooß, J. U., Brühl, C., Russel III, J. M. and co-authors. 1996. Chlorine activation and ozone depletion in the Arctic vortex: Observations by the Halogen Occultation Experiment on the Upper Atmosphere Research Satellite. *J. Geophys. Res.* **101**, 12531–12554.

Murphy, D. M., Thomson, D. and Mahoney, M. J. 1998. In situ measurements of organic meteoric material, mercury, and other elements in aerosols at 5 to 19 kilometers. *Science* **282**, 1664–1669.

Nedoluha, G. E., Bevilacqua, R. M., Hoppel, K. W., Daehler, M., Shettle, E. P. and co-authors. 2000. POAM III measurements of dehydration in the Antarctic lower stratosphere. *Geophys. Res. Lett.* **27**, 1683–1686.

Nedoluha, G. E., Bevilacqua, R. M. and Hoppel, K. W. 2002. POAM III measurements of dehydration in the Antarctic and comparisons with the Arctic. *J. Geophys. Res.* **107**, 8290, doi:10.1029/2001JD001184.

Ovarlez, J., Gayet, J. F., Gierens, K., Ström, J., Ovarlez, H. and co-authors. 2002. Water vapour measurements inside cirrus clouds in Northern and Southern hemispheres during INCA. *Geophys. Res. Lett.* **29**, doi:10.1029/2001GL014440.

Pan, L. L., Randel, W. J., Nakajima, H., Massie, S. T., Kanzawa, H. and co-authors. 2002. Satellite observation of dehydration in the Arctic polar stratosphere. *Geophys. Res. Lett.* **29**, doi:10.1029/2001GL014147.

Petzold, A., Ström, J., Ohlsson, S. and Schröder, F. P. 1998. Elemental composition and morphology of ice crystal residual particles in cirrus clouds and contrails. *Atmos. Res.* **49**, 21–34.

Petzold, A., Hoell, C., Kärcher, B., Beuermann, B., Schiller, C. and co-authors. 2000. In situ observations of aerosol properties above ice saturation in the polar tropopause region. *J. Geophys. Res.* **195**, 29,387–29,395.

Proffitt, M. H., Margitan, J. J., Kelly, K. K., Loewenstein, M., Podolske, J. R. and co-authors. 1990. Ozone loss in the Arctic polar vortex inferred from high altitude aircraft measurements. *Nature* **347**, 31–36.

Read, W. G., Wu, D. L., Waters, J. W. and Pumphrey, H. C. 2004. Dehydration in the tropical tropopause layer: implications from the UARS Microwave Limb Sounder. *J. Geophys. Res.* **109**(D6), D06119, doi:10.1029/2003JD004056.

Reiter, E. R. 1975. Stratospheric-tropospheric exchange processes. *Rev. Geophys. Space Phys.* **13**, 459–474.

Sassen, K. 2005. Dusty ice clouds over Alaska. *Nature* **434**, 456.

Scheeren, H. A., Fischer, H., Lelieveld, J., Hoor, P., Rudolph, J. and co-authors. 2003. Reactive organic species in the northern extratropical lowermost stratosphere: Seasonal variability and implications for OH. *J. Geophys. Res.* **108**(D24), 4805, doi:10.1029/2003JD003650.

Schiller, C., Afchine, A., Eicke, N., Feigl, C., Fischer, H. and co-authors. 1999. Ice particle formation and sedimentation in the tropopause region: A case study based on in situ measurements of total water during POLSTAR 1997. *Geophys. Res. Lett.* **26**, 2219–2222.

Schiller, C., Bauer, R., Cairo, F., Deshler, T., Dörnbrack, A. and co-authors. 2002. Dehydration in the Arctic stratosphere during the

SOLVE/THESEO-2000 campaigns. *J. Geophys. Res.* **107**, 8293, doi:10.1029/2001JD000463.

Shapiro, M. A. 1980. Turbulent mixing within tropopause folds as a mechanism for the exchange of chemical constituents between stratosphere and troposphere. *J. Atmos. Sci.* **37**, 994–1004.

Ström, J. and Ohlsson, S. 1998. In situ measurements of enhanced crystal number densities in cirrus clouds caused by aircraft exhaust. *J. Geophys. Res.* **103**, 11 355–11 361.

Ström, J., Seifert, M., Kärcher, B., Ovarlez, J., Minikin, A. and coauthors. 2003. Cirrus cloud occurrence as function of ambient relative humidity: a comparison of observations obtained during the INCA experiment. *Atmos. Chem. Phys.* **3**, 1807–1816.

Tabazadeh, A., Jensen, J. and Toon, O. B. 1997a, A model description of cirrus cloud nucleation from homogeneous freezing of sulfate aerosols. *J. Geophys. Res.* **102**, 23 845–23 850.

Tabazadeh, A., Toon, O. B. and Jensen, E. J. 1997b, Formation and implications of ice particle nucleation in the stratosphere. *Geophys. Res. Lett.* **24**, 2007–2010.

Vömel, H., Oltmans, S. J., Hoffmann, D. J., Deshler, T. and Rosen, J. M. 1995. The evolution of the dehydration in the Antarctic stratospheric vortex. *J. Geophys. Res.* **100**, 13 919–13 926.

Vömel, H., Rummukainen, M., Kivi, R., Karhu, J., Turunen, T. and coauthors. 1997. Dehydration and sedimentation of ice particles in the Arctic stratospheric vortex. *Geophys. Res. Lett.* **24**, 798–798.

Zöger, M., Schiller, C. and Eicke, N. 1999. Fast in situ hygrometers: a new family of balloonborne and airborne Lyman-α photofragment fluorescence hygrometers. *J. Geophys. Res.* **104**, 1807–1816.